ACS Energy LETTERS

http://pubs.acs.org/journal/aelccp

PERSPECTIVE

# Charge-Carrier Mobilities in Metal Halide Perovskites: Fundamental Mechanisms and Limits

Laura M. Herz*

Department of Physics, University of Oxford, Clarendon Laboratory, Parks Road, Oxford OX1 3PU, U.K.

**ABSTRACT:** **Perovskite photovoltaic cells have seen a remarkable rise in power conversion efficiencies over a period of only a few years. Much of this performance is underpinned by the favorable charge-carrier mobilities in metal halide perovskites (MHPs), which are remarkably high for materials with such facile and versatile processing routes. This Perspective outlines the mechanisms that set a fundamental upper limit to charge-carrier mobility values in MHPs and reveals how they may be tuned through changes in stoichiometry. In addition, extrinsic effects such as grain size, energetic disorder, and self-doping are discussed for specific MHPs in the context of remedies designed to avoid them.**

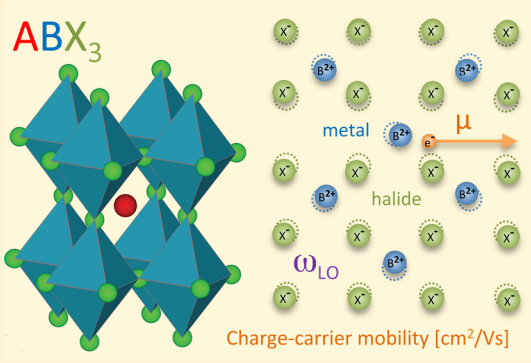


Metal halide perovskites (MHPs) have ushered in an exciting new period of "perovskite photovoltaics" with certified power conversion efficiencies now exceeding 20% following only a few years of active development.[1] The fundamental semiconducting properties that make MHPs such outstanding light harvesters and charge conductors have been summarized in several recent reviews.[2−4] Strong interband transitions offer large absorption coefficients[5,6] and bimolecular recombination significantly below the Langevin limit,[7] while a benign defect chemistry[8,9] yields low trap-related recombination rates[3,10] for the charge-carrier density regimes typically encountered under solar illumination conditions.[11] Together with typical charge-carrier mobility values in the tens of $cm^2/(V\,s)$ for thin films of lead iodide perovskites, these properties have led to long charge-carrier diffusion lengths in the micrometer range under solar illumination densities,[10−12] which has paved the way for the thin-film photovoltaic device architectures now typically employed.[13−15]

Despite such progress in fundamental understanding and device performance, one issue still puzzling the community is the mechanisms limiting charge-carrier mobilities in MHPs. The ratio of charge-carrier mobility and recombination rate critically influences the charge-carrier diffusion length, and while trap-related recombination rates are readily assessed, an understanding of charge-carrier mobilities is only just emerging. As pointed out in a recent contribution,[16] charge-carrier mobilities in MHPs should really be compared with those of typical inorganic ionic semiconductors, such as GaAs, which displays only slightly lower effective masses for conduction band electrons and valence band holes but substantially higher mobilities.

Charge-carrier mobilities in MHPs should really be compared with those of typical inorganic ionic semiconductors, such as GaAs.

Mechanisms that limit the charge-carrier mobility in MHPs can conveniently be divided into extrinsic and intrinsic effects. Intrinsic effects result from charge-carrier interactions with the underlying lattice that cannot be avoided. An understanding of such effects will allow for improved modeling from first principles that may permit the design of high-charge-mobility MHPs based on the $ABX_3$ stoichiometry. Extrinsic effects, on the other hand, are limited by material imperfections, such as grain boundaries, energetic disorder, or impurities that may be avoided through suitable material processing. A clear knowledge of the mechanisms governing intrinsic charge-carrier conduction will therefore also allow the setting of realistic goals as to what can be achieved through improved processing strategies.

This Perspective aims to clarify the current state of the debate surrounding charge-carrier mobilities in MHPs. A survey of the current literature is first provided to allow comparison of charge-carrier mobilities extracted from a host of different measurement techniques, whose inherent uncertainties can result in a substantial variation of values obtained, even for the same sample.[17,18] The intrinsic factors limiting charge-carrier mobi-

**Received:** March 29, 2017
**Accepted:** May 31, 2017
**Published:** May 31, 2017

  

DOI: 10.1021/acsenergylett.7b00276
*ACS Energy Lett.* 2017, 2, 1539−1548

Table 1. Charge-Carrier Mobility Values at Room Temperature, Determined Experimentally for MHPs[a]

| MHP | architecture | fabric. route | measurement | electron, hole, sum | mobility $cm^2(V\,s)^{-1}$ | ref. |
|---|---|---|---|---|---|---|
| $MAPbI_3$ | film | sol. | THzC | Σ | 35 | 19 |
| | film | sol. | THzC | Σ | 20 | 20 |
| | film | sol. | MWC | Σ | 30 | 21 |
| | film | sol. | MWC | Σ | 29 | 22 |
| | film | sol. | MWC | Σ | 71 | 23 |
| | film | sol. | PLQ | e | 1.4 | 12 |
| | film | sol. | PLQ | h | 0.9 | 12 |
| | film | sol. | PLQ | e | 0.7 | 10 |
| | film | sol. | PLQ | h | 0.4 | 10 |
| | film | sol. | micros | e/h | 2−3 | 24 |
| | meso | sol. | THzC | Σ | 8 | 7 |
| | meso | sol. | MWC | Σ | 9 | 21 |
| | singleC | sol. | SCLC | h | 164 | 18 |
| | singleC | sol. | SCLC | h | 67 | 25 |
| | singleC | sol. | SCLC | h | 2.5 | 17 |
| | singleC | sol. | THzC | Σ | 600 | 26 |
| | singleC | sol. | MWC | Σ | 115 | 27 |
| | singleC | sol. | TOF | h | 24 | 18 |
| | singleC | sol. | Hall | h | 105 | 18 |
| | polyC | var. | Hall | e | 66 | 28 |
| $MAPbI_{3-x}Cl_x$ | film | vap. | THzC | Σ | 33 | 29 |
| | film | sol. | THzC | Σ | 27 | 30 |
| | film | sol. | MWC | Σ | 27 | 21 |
| | film | sol. | PLQ | e | 1.6 | 10 |
| | film | sol. | PLQ | h | 2.1 | 10 |
| | meso | sol. | THzC | Σ | 12 | 7 |
| | meso | sol. | MWC | Σ | 7.5 | 21 |
| $FAPbI_3$ | film | sol. | THzC | Σ | 27 | 31 |
| | film | sol. | PLQ | e | 0.2 | 32 |
| | film | sol. | PLQ | h | 3.5 | 32 |
| | singleC | sol. | SCLC | h | 35 | 33 |
| | singleC | sol. | SCLC | | 4.4 | 34 |
| $Cs_{0.17}FA_{0.83}PbI_3$ | film | sol. | THzC | Σ | 40 | 35 |
| $MAPbBr_3$ | film | v/a | PLQ | e | 8.6 | 36 |
| | film | v/a | PLQ | h | 9.0 | 36 |
| | singleC | sol. | SCLC | h | 24 | 25 |
| | singleC | sol. | SCLC | h | 38 | 17 |
| | singleC | sol. | Hall | h | 40 | 17 |
| | singleC | sol. | TOF | h | 115 | 17 |
| $FAPbBr_3$ | film | sol. | THzC | Σ | 14 | 31 |
| | singleC | sol. | SCLC | h | 62 | 33 |
| $Cs_{0.17}FA_{0.83}PbBr_3$ | film | sol. | THzC | Σ | 11 | 35 |
| $MAPbCl_3$ | singleC | sol. | SCLC | h | 42 | 37 |
| $FAPb(Br_xI_{1-x})_3$ | film | sol. | THzC | Σ | 1−27 | 31 |
| $Cs_yFA_{1-y}Pb(Br_{0.4}I_{0.6})_3$ | film | sol. | THzC | Σ | 4−21 | 35, 38 |
| $Cs_{0.17}FA_{0.83}Pb(Br_xI_{1-x})_3$ | film | sol. | THzC | Σ | 11−40 | 35, 39 |
| $MASnI_3$ | meso | sol. | THzC | Σ | 1.6 | 40 |
| | polyC | sol. | Hall | h | 50 | 41 |
| | singleC | sol. | Hall | h | 200 | 42 |
| | polyC | var. | Hall | h | 322 | 28 |
| | polyC | var. | Hall | e | 2320 | 28 |
| $FASnI_3$ | film | sol. | THzC | Σ | 22 | 43 |
| | polyC | var. | Hall | e | 103 | 28 |
| $CsSnI_3$ | polyC | var. | Hall | e | 536 | 28 |
| | polyC | ss | Hall | h | 585 | 44 |
| $MASn_{0.5}Pb_{0.5}I_3$ | polyC | var. | Hall | e | 270 | 28 |
| $FASn_{0.5}Pb_{0.5}I_3$ | film | sol. | THzC | Σ | 17 | 14 |
| $Cs_{0.25}FA_{0.75}Sn_{0.5}Pb_{0.5}I_3$ | film | sol. | THzC | Σ | 14 | 14 |
| $(C_6H_5C_2H_4NH_3)_2SnI_4$ | film(2D) | sol. | FET | h | 0.6 | 45 |
| $PEASnI_4$ | film(2D) | sol. | FET | h | 15 | 46 |
| $MA_{n-1}PEA_2Pb_nI_{3n+1}$ | film(2D) | sol. | THzC | Σ | 6−11 | 47 |



DOI: 10.1021/acsenergylett.7b00276
ACS Energy Lett. 2017, 2, 1539−1548

**Table 1. continued**

[a]Column 1 states the chemical formulae, where MA is $CH_3NH_3$ (methylammonium), FA is $HC(NH_2)_2$ (formamidinium), and PEA is 2-phenylethylammonium. Column 2 lists the material architecture (thin *film*; *meso*, infusion into a mesoporous metal oxide matrix; *singleC*, single crystal; *polyC*, poly-crystal; *film(2D)*, thin film of layered (2D) MHP. Column 3 indicates the fabrication route, (*sol.*, e.g. spin-coating of thin films or cyrstal growth from solution; *vap.*, thin-film deposition from vapor phase; *v/a*, vapor-assisted route; *ss*, solid-state synthesis; *var.*, various methods). Column 4 lists the technique used to deterimine the mobility value (*THzC*, optical-pump-THz-probe photoconductivity; *MWC*, microwave conductivity; *PLQ*, PL quenching method; *micros*, optical microscopy; *SCLC*, space-charge limited current; *Hall*, Hall coefficient and resistivity measurements; *TOF*, time-of-flight transients; *FET*, field-effect-transistor mobility). Column 5 indicates whether mobility values are for conduction-band electrons (e), valence-band hole (h), or the sum (Σ) over both. Column 6 lists the charge-carrier mobility values reported in the literature studies referenced in column 7.

lities of MHPs are then clarified, with an outlook given on how MHP composition must consequently be tailored to allow for high charge-carrier mobilities. Finally, extrinsic factors limiting charge-carrier mobilities in specific MPHs are considered, including the effect of grain size in lead halide perovskites, the presence of energetic disorder in highly doped tin iodide perovskites, structural disorder in alloyed mixed-halide lead halide perovskites, and effects arising from confinement in quasi-two-dimensional (quasi-2D) MHPs.

*Experimentally Determined Values for Charge-Carrier Mobilities in MHPs.* Table 1 provides a literature overview of charge-carrier mobilities measured for $ABX_3$ perovskites, for A= MA (methylammonium), FA (formamidinium), Cs; B = Pb, Sn; and X = I, Br, Cl, and alloys thereof. In addition, a few examples of layered (quasi-2D) perovskites are provided. It is noticeable that

> It is noticeable that for any given stoichiometry, reported charge-carrier mobility values encompass a considerable range.

for any given stoichiometry, reported charge-carrier mobility values encompass a considerable range. As a first approach, one might consider this variation to arise from differences in fabrication techniques and the ensuing material morphologies. However, the range of reported values is particularly wide for single-crystal samples, which suggests that systematic or statistical errors associated with different measurement techniques are largely to blame. For thick single crystals, in particular, measurements can be challenging to conduct and analyze, relying for example on electrical-current extraction or terahertz (THz) conductivity probes in reflection geometry. In addition, different techniques reflect subtly different spatial ranges, with relatively local charge-carrier motion being probed in high-frequency conductivity measurements that are therefore less affected by grain boundaries than long-range current-extraction or charge-carrier diffusion experiments. Variations in experimentally determined parameters are a fundamental fact of nature. Through repeated reporting the field will eventually converge on a better understanding of what can typically be expected for a given stoichiometry and morphology. However, at the present stage, the wide ranges reported demonstrate that a value returned from any single measurement must be treated with some care.

Both electrical and noncontact probes have been used to investigate charge-carrier mobilities in MHPs. *Space-charge-limited-current (SCLC)* techniques have frequently been employed,[17,18,25,33,37] which monitor current extraction as a function of bias voltage for crystals sandwiched between two metal electrodes. If a clear trap-independent space-charge-limited regime is reached at high voltages, the charge-carrier mobility may be extracted from the Mott−Gurney law. *Hall effect* measurements[17,18,28,41,42,44] rely on deflection of charge carriers in a magnetic field that leads to a charge build-up, or Hall voltage, from which the charge-carrier density can be extracted. Because the direction of deflection is also monitored, a differentiation between conducting electrons and holes can readily be made. Combination with electrical resistivity measurements allows for a charge-carrier mobility to be determined, whose accuracy may be affected if both measurements are not conducted on identical samples.[28] In addition, the *time-of-flight technique (TOF)* may be used to assess charge-carrier mobilities. Here the transient current through the device is monitored following a voltage pulse. If a clear transit time can be identified, the mobility can be extracted under knowledge of the thickness traveled. All such device measurement also tend to be influenced by the quality and type of electrical contact made. In addition, the prolonged application of low-frequency or DC electrical fields to MHPs has been shown to cause slow ionic migration, in particular of the halide ions,[48,49] which could potentially influence results.

Noncontact probes of AC conductivity can potentially circumvent some of these problems, but they are more complex to implement and analyze. Optical-pump-THz-probe measurements of *electrical conductivity at THz frequency (THzC)* following photoexcitation with a short optical pulse have been used repeatedly to monitor the charge-carrier mobility of MHPs.[7,14,19,20,26,29,31,35,38−40] Extraction of THz charge-carrier mobilities for thin MHP films is readily achieved using, for example, a thin-film optical model[29] to convert the initial change in photoinduced transmission of THz radiation. However, THzC measurements and analysis for thick single crystals is significantly complicated by the need for reflection geometries and careful accounting for competing lattice absorption features.[26] A similar method is the *transient microwave conductivity (MWC)* technique which monitors the change in Q-value of a microwave cavity containing a sample after it has been photoexcited by a nanosecond pulse.[20−22]

In an alternative approach, values of the charge-carrier mobility $\mu$ may be derived from measurements of the diffusion coefficient $D$, using the relation $\mu = eD/(k_BT)$ which yields $\mu = 38.9\ V^{-1}\ D$ at room temperature. Diffusion coefficients have frequently been extracted from *photoluminescence quenching (PLQ)* methods[10,12,32,36] where PL transients are monitored following the photoexcitation of a thin MHP film that forms an interface with an electron or hole extraction layer. Such measurements are easy to conduct, allow differentiation between electron and hole mobilities, and probe charge motion through the whole film depth profile, which bears resemblance to charge extraction in a typical solar cell. However, modeling of the results relies on accurate knowledge of the charge-transfer efficiency at the interface,[50] which is often assumed to be unity for simplicity. Another possibility is the direct monitoring of charge-carrier diffusion through *microscopy*, by following over time the lateral



DOI: 10.1021/acsenergylett.7b00276
ACS Energy Lett. 2017, 2, 1539−1548

spread of a charge-carrier density distribution, generated by a Gaussian laser profile.[24] Such techniques do not require the presence of an extractor layer and allow for high spatial resolution; however, they probe charge-carrier motion in the plane of the film.

Because the charge-carrier mobility values shown in Table 1 vary between studies, it is more representative to assess averages and the associated standard deviation for MHPs with sufficient available data. $MAPbI_3$ and its near-equivalent $MAPbI_{3-x}Cl_x$ have been particularly well investigated, which allows for a comparison of different morphologies. Thin-film experiments here yield average sum carrier mobilities of $(2.4 \pm 1.1)$ $cm^2/(V\,s)$ for long-range PLQ measurements and average values of $(37 \pm 18)$ $cm^2/(V\,s)$ for short-range THz and microwave conductivity probes, suggesting a lingering effect of grain boundaries on transport.

For single-crystal MHPs, reported charge-carrier mobilites tend to be higher than those for thin films, although not spectacularly so. Accurate assessment here is complicated by the strong variations in values provided by different studies for the same MHP. For example, Table 1 shows that for single-crystalline $MAPbI_3$ alone, reports range between a value of 2.5 $cm^2/(V\,s)$ for the hole mobility and 600 $cm^2/(V\,s)$ for the electron–hole sum mobility, which constitutes about 2 orders of magnitude in discrepancy. Given that identical single crystals of the same stoichiometry and structure should return the same charge-carrier mobility, this vast range must be almost entirely caused by experimental uncertainty. To partly alleviate these effects, average values may be calculated over multiple results for the hole mobilities in $MAPbI_3$ ($73 \pm 58$ $cm^2/(V\,s)$), $MAPbBr_3$ ($54 \pm 36$ $cm^2/(V\,s)$), and $MASnI_3$ ($191 \pm 111$ $cm^2/(V\,s)$). While these average values need to be taken with care, considering the large standard deviations from the mean, they suggest that the hole mobility declines from iodide to bromide and increases from lead to tin-based perovskites. For single crystals, such changes should reflect modifications in the fundamental mechanism limiting charge-carrier mobilities in MHPs, the origin of which will be discussed below.

*Intrinsic Factors Limiting Charge-Carrier Mobilities in MHPs.* Discussion of the fundamental limits posed to the charge-carrier mobility in MHPs have mostly focused on $MAPbI_3$ because its defect chemistry is particularly benign,[8,9] allowing facile fabrication of thin films with high crystallinity and long charge-carrier diffusion lengths in excess of micrometers.[10,18] Early investigations showed that the low-frequency charge-carrier mobility in $MAPbI_3$ increases strongly with decreasing temperature[19,51,52] in accordance with a suppression of interactions between electrons and lattice vibrations (phonons) as their mode occupancy is reduced. In addition, photoconductivity spectra were Drude-like, implying the absence of strong scattering from crystalline boundaries.[7,26,29] Such observations suggest that the charge-carrier mobility in $MAPbI_3$ is already approaching the intrinsic limit. Room-temperature values of $(37 \pm 18)$ $cm^2/(V\,s)$ for the short-range electron–hole sum mobility in high-quality thin films and $(73 \pm 58)$ $cm^2/(V\,s)$ for holes in single crystals therefore serve as a benchmark to any investigation of the underlying charge-carrier scattering mechanisms.

Within the simple Drude picture,[53] the charge-carrier mobility $\mu$ in a conductor is determined by only two factors, the effective mass of the electron ($m_e^*$) or hole ($m_h^*$) and the momentum relaxation time $\tau$, with $\mu = e\tau/m^*$. Here, random scattering events occurring at average time intervals $\tau$ lead to intermittent randomization of a charge-carrier's velocity with respect to the direction of the electric field, and therefore Ohmic conduction. The effective masses of charge-carriers are relatively easily assessed, either from first-principles calculations of the band curvature[54−59] or through experimental techniques such as magneto-absorption measurements.[60−63] Such evaluations agree that effective electron and hole masses in $MAPbI_3$ are relatively similar and $\sim 0.1-0.2 m_e$, where $m_e$ is the free-electron mass. Variation of perovskite stoichiometry will lead to subtle changes in band curvature, which will be reflected in altered effective charge-carrier masses and therefore mobilities.[57,64] Based on the above-mentioned values of the effective masses, charge-carrier mobility values of <100 $cm^2/(V\,s)$ for $MAPbI_3$ would require momentum relaxation times below 10 fs, much shorter than those for GaAs, for which scattering times of several hundred femtoseconds can be derived from the room-temperature hole- and electron-mobility (450 and 9000 $cm^2/(V\,s)$, respectively).[65] These simple considerations suggest that the lower charge-carrier mobility in $MAPbI_3$ is mostly attributable to higher electron–phonon coupling.

The interaction of charge-carriers with crystal vibrations is generally described within two main categories. Deformation potential scattering[53,66,67] involves a temporary distortion of the lattice which changes the band structure and therefore couples the electronic and vibrational states. For polar interactions, on the other hand, electrons are affected by the electric fields caused by a polarization of the ionic lattice. Such polarization may be mediated by a piezoelectric effect resulting from the strain caused by a lattice vibration (piezoelectric acoustic phonon scattering) or by Fröhlich interactions[53,68,69] involving the macroscopic electric field generated by a longitudinal optical (LO) phonon. It has been argued[70,71] that both the optical-phonon deformation potential and the piezoelectric acoustic-phonon scattering terms vanish for the $Pm\bar{3}m$ reference structure of $MAPbI_3$. Therefore, a primary assessment of electron–phonon coupling in $MAPbI_3$ requires the correct evaluation of both acoustic-phonon deformation potential (ADP) scattering and of Fröhlich interactions with LO phonons.

Ab initio calculations have suggested that acoustic-phonon deformation-potential scattering is relatively weak for $MAPbI_3$ and should result in charge-carrier mobilities of several thousand $cm^2/(V\,s)$ at room temperature if it were the sole mechanisms in operation.[72,73] Inclusion of Rashba effects in such calculations reduces the expected charge-carrier mobility somewhat,[74] but not to the values <100 $cm^2/(V\,s)$ experimentally encountered at room temperature. From a theoretical perspective, ADP scattering is therefore unable to account for the observed mobility values. In spite of this, one experimental study[30] postulated a dominance of ADP scattering because the $T^{-1.5}$ temperature dependence of the charge-carrier mobility in $MAPbI_3$ measured by several groups[19,30,51,52] happens to follow the simplified result derived for noninteracting phonon modes associated with a harmonic lattice potential.[53,66,67] However, as pointed out subsequently in several other studies,[74−78] this classical result is highly unlikely to apply to $MAPbI_3$, given the presence of multiple atoms per unit cell, large number of phonon modes, phonon anharmonicity,[78,79] and dynamic disorder. An experimental study by Wright et al. evaluated the contribution of ADP scattering to the line shape broadening of luminescence in the related $FAPbI_3$ and found it to make only a minor contribution to the overall electron–phonon coupling at room temperature.[75] Hence, the theoretical and experimental studies broadly agree that acoustic phonon deformation potential



DOI: 10.1021/acsenergylett.7b00276
ACS Energy Lett. 2017, 2, 1539−1548

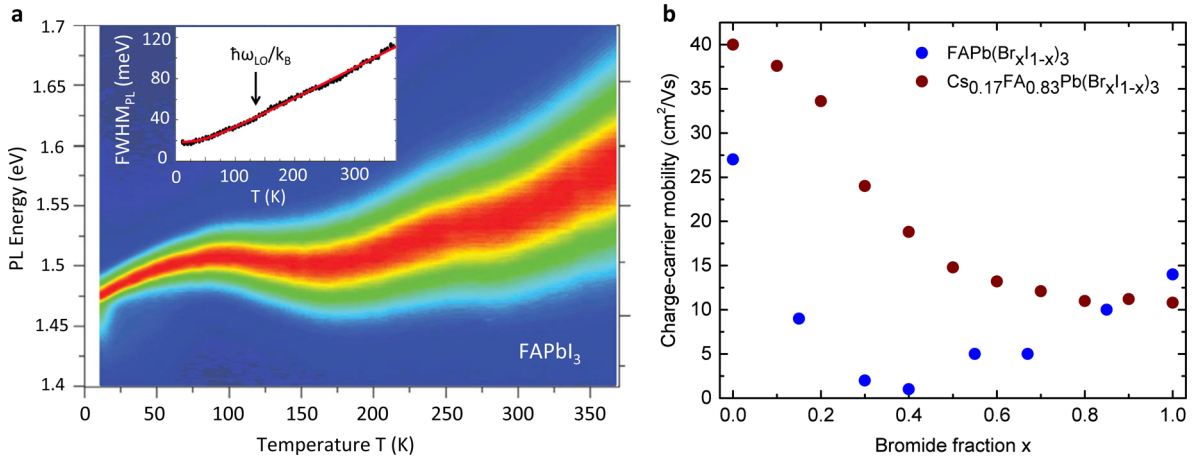


**Figure 1. (a) Color plot of normalized steady-state photoluminescence spectra for a $FAPbI_3$ thin film at temperatures between 10 and 370 K. The inset shows the full width at half-maximum (FWHM) of the PL peak versus temperature, with the arrow indicating the characteristic temperature coresponding to the main LO phonon mode involved in the Fröhlich interactions (adopted from ref 75). (b) Room-temperature charge-carrier mobility as a function of bromide fraction $x$ for $FAPb(Br_xI_{1-x})_3$ (data taken from ref 31) and $Cs_{0.17}FA_{0.83}Pb(Br_xI_{1-x})_3$ (data taken from ref 35). The "mobility gap" resulting from an instability in the crystal structure is remedied when a small fraction of cesium is substituted for FA.**

scattering cannot be the dominant factor limiting the room-temperature charge-carrier mobility in $MAPbI_3$.

Experimental evidence for the presence of polar scattering mechanisms was provided by a study[75] of the temperature-dependent emission broadening in $FAPbI_3$, which (unlike $MAPbI_3$)[80] exhibits "clean" phase transitions that are not complicated by inclusions of different crystal structure (see Figure 1a). Electron−phonon coupling was found to be markedly reduced below the characteristic temperature corresponding to the energy of the relevant LO phonon (11 meV),[81] in agreement with Fröhlich interactions being the dominant mechanisms at room temperature.[75] Recent ab initio calculations including Fröhlich coupling confirm this to have a dominant effect at room temperature, yielding charge-carrier mobility values near 100 $cm^2/(V\ s)$ and correctly reproducing the experimentally observed temperature dependence.[74,76,82] Therefore, the $T^{-1.5}$ temperature dependence of the charge-carrier mobility in the high-temperature regime appears to result directly from the given range of LO phonons and Fröhlich coupling strengths present in this specific system (lead iodide perovskite). Substantial stoichiometric changes, for example, through substitution with a lighter atom, may well result in different temperature dependences.

It is not surprising that Fröhlich interactions are the dominant mechanism limiting charge-carrier mobility in $MAPbI_3$ at room temperature, given that this has mostly been the case for polar semiconductors, including GaAs.[53,83] The relatively polar nature of the lead-halide bond[84] is reflected by sizable Born effective charges[75] and wide Reststrahlen bands[77] that lead to a large Fröhlich coupling constant. In addition, the relatively low energy of relevant LO phonon modes in $MAPbI_3$ (~11 meV)[81] compared with GaAs (~31 meV)[85] causes the Fröhlich mechanism to onset at lower temperature and therefore to contribute more strongly at room temperature (see Figure 1a). Hence, the lower room-temperature mobility of charge-carriers in $MAPbI_3$ in comparison to GaAs can be largely understood in terms of enhanced Fröhlich effects.

It is not surprising that Fröhlich interactions are the dominant mechanism limiting charge-carrier mobility in $MAPbI_3$ at room temperature, given that this has mostly been the case for polar semiconductors, including GaAs.

Such analysis allows broader predictions of how fundamental limits to the charge-carrier mobility can be tuned through MHP composition. Because the Fröhlich interaction strength depends critically on the high- and low-frequency limits of the dielectric function and on the LO phonon frequency,[53,68,69] such experimentally accessible parameters can be used to predict mobility trends. For example, Fröhlich interactions were found to be enhanced in $APbBr_3$ with respect to $APbI_3$ (for A = MA, FA), which was attributed to the higher ionicity of the Pb−Br bond with respect to the Pb−I bond.[75] These observations may explain the higher charge-carrier mobilities often observed for $APbI_3$ with respect to $APbBr_3$ films fabricated under similar procedures.[31,35] Sendner et al. used such arguments to derive charge-carrier mobility values for single crystals of $MAPbX_3$ (X = Cl, Br, I) from infrared reflectivity spectra alone, which allow for extraction of TO and LO phonon mode energies and low- and high-frequency values of the dielectric function.[77] This approach yielded upper limits to the room-temperature mobility (i.e., under the assumption of sole Fröhlich contributions) that declined across the halide series from 197 $cm^2/(V\ s)$ for $MAPbI_3$ to 58 $cm^2/(V\ s)$ for $MAPbCl_3$, again as a result of the increased ionicity of the lead-halide bond. Similarly, the Fröhlich coupling mechanism can explain the significant differences in charge-carrier mobility between tin- and lead-based MHPs, reflected in Table 1 (beyond those arising from simple changes in effective charge-carrier masses[57]). Within the Fröhlich approach,[86,87] the charge-carrier mobility falls with increasing temperature $T$ as a function of the dimensionless parameter $\beta = \hbar\omega_{LO}/k_BT$. Use of the lighter element tin will lead to an upshift in LO phonon frequencies $\omega_{LO}$, which scales such mobility curves to higher temperatures; thus, the room-temperature mobility is enhanced. Therefore, careful evaluation of Fröhlich electron−phonon coupling for MHPs, through factors such as the ionicity of metal-halide bonds and the frequency of the contributing LO phonon branches, can provide realistic upper limits to charge-



DOI: 10.1021/acsenergylett.7b00276
ACS Energy Lett. 2017, 2, 1539−1548

carrier mobilities that can be reached once all extrinsic factors are eliminated.

Finally, the dominance of Fröhlich effects must also be rationalized in terms of its polaronic description. As pointed out by both Fröhlich[68] and Feynman,[69] the placement of a mobile electron in the ionic lattice polarizes its neighborhood, giving rise to the polarization field that creates the Fröhlich interaction. Because it carries the polarization field with it through the crystal, the electron is slowed, which lowers its mobility and effective mass. Such effects are still fully compatible with a band structure picture, provided that the radii of such polarons are much larger than the lattice constant. Recent calculations have suggested that such radii are indeed of the order of 40−50 Å in $MAPbI_3$, which satisfies this criterion.[74,77] In addition, effective masses of such large polarons were calculated to be higher by only 20−36% with respect to the free-charge masses, making this picture still fully compatible with experimentally determined values.[54−63] The existence of large polarons is also in line with the observed increase in charge-carrier mobility with decreasing temperature, as calculated by Feynman[69,88] and observed for various ionic materials such as $Bi_{12}SiO_{20}$,[86] GaAs,[83] and $MAPbI_3$.[19,30,51,52] However, the presence of highly localized "small" polarons in $MAPbI_3$, as recently postulated,[71] would be hard to reconcile with the above-mentioned observations, as it ought to lead to temperature-activated hopping transport and heavy effective masses that are not experimentally observed for $MAPbI_3$.

*Extrinsic Factors Influencing the Charge-Carrier Mobilities in MHPs.* While intrinsic electron−phonon coupling may set a limit to the maximum attainable charge-carrier mobilities for any given MHP, these limits are not usually fully achieved for thin films.

> Charge-carrier mobilities are frequently lowered through extrinsic mechanisms, including charge-carrier scattering by grain boundaries, dopants, and a disordered energy landscape.

Charge-carrier mobilities are frequently lowered through extrinsic mechanisms, including charge-carrier scattering by grain boundaries, dopants, and a disordered energy landscape. An understanding of such effects has been at the core of MHP research, with protocols being developed that allow for optimized charge-carrier mobilities and therefore diffusion lengths. Below, a summary is given of some recent findings and remedies regarding extrinsic factors lowering the charge-carrier mobility in MHPs.

Grain size is clearly still one factor limiting charge-carrier mobilities in MHPs, as evident from the lowering of charge-carrier mobility values determined when moving from single crystals to thin films and from short-range to long-range measurements (see Table 1). Similarly, early studies found that long- and short-range charge-carrier mobilities and diffusion lengths were significantly enhanced[7,10] in $MAPbCl_xI_{3-x}$ compared to $MAPbI_3$. These differences were attributed to the higher crystallinity and more benign grain boundaries of the former material,[89] which has an insignificant amount of chloride actually included in the structure.[90,91] In addition, MHPs infiltrated into mesoporous matrices such as $Al_2O_3$ nanoparticles form smaller grains and exhibit lower charge-carrier mobilities than in equivalent planar thin-film architectures.[7,19,21] Measurements of gigahertz charge-carrier mobility[22] in $MAPbI_3$ and THz charge-carrier mobility[39] in $FA_{0.83}Cs_{0.17}Pb(Br_{0.2}I_{0.8})_3$ revealed a systematic increase with grain size that plateaued once grains exceeded the size beyond which scattering off boundaries became negligible. Grain size is thus still a factor limiting charge-carrier conduction even in thin films of high-quality MHPs such as $MAPbI_3$. However, room-temperature mobility values obtained for such materials are now often less than an order of magnitude below the intrinsic limits discussed above (see Table 1), which is an amazing feat for materials with such versatile and facile processing routes.

In tin-based perovskites, doping and impurities are a major factor currently limiting the charge-carrier mobility because these materials suffer from a $Sn^{2+}$ to $Sn^{4+}$ oxidation route that induces electrical hole doping[40−43] at densities as high as $10^{17}$−$10^{19}$ $cm^{-3}$. Because overall charge neutrality requires the remnant hole dopant site to be negatively charged, it will act as a scattering site to charge-carriers, as evident, for example, in temperature-dependent emission-line broadening measurements[92] in $MASnI_3$. Such effects are well-known for classic inorganic semiconductors such as GaAs, for which electrical doping is therefore preferably implemented by moving the dopant impurities away from the charge-conduction region (e.g., through modulation doping).[93,94] One proposed remedy for such effects has been treatment with $SnF_2$ to reduce the background carrier density in tin-iodide perovskites.[95,96] However, such treatments can induce a complex variety of changes that still require further understanding. Such doping-induced reduction of charge-carrier mobility can in principle occur in any hybrid perovskite, including lead iodide materials.[97] However, in tin-based perovskites, the B-metal oxidation route has a particularly low hurdle, which typically results in charge-carrier scattering with impurities dominating over intrinsic factors.

Aside from charge-impurity scattering, a severely disordered energy landscape appears to be a major factor limiting the charge mobility in tin-based MHPs. Sizeable Stokes shifts near 200 meV between the absorption onsets and emission peaks were found for $MASnI_3$ films[92] which display THz charge-carrier mobilities[40] near 2 $cm^2/(V\ s)$, orders of magnitude below any values determined for single crystals (see Table 1). A marked improvement was reported for $FAPbI_3$ thin films,[43] with Stokes shifts reduced to 60 meV, and charge-carrier mobilities as high as 22 $cm^2/(V\ s)$, sufficient to allow fabrication of planar-heterojunction photovoltaic devices.[14] The energetically broadened landscape in tin-based MHP films may also be related to their propensity to self-dope, reminiscent of similar effects in copper zinc tin sulfide (CZTS) kesterites, where charged defects can lead to potential fluctuations resulting in tail states that protrude into the band gap.[98,99]

Energetic disorder also frequently limits charge-carrier mobilities in MHP alloys that fall outside the stable crystallographic range. For the commonly explored $(MA/FA/Cs)Pb(Br/I)_3$ perovskite system, regions of structural instability exist that have been attributed to effective ionic radii that are incompatible with the Goldschmidt[100] tolerance factor[38,101,102] or to structural transitions that occur with progressing alloy fraction.[32] For example, significant energetic disorder for intermediate ($x \approx 0.3$−$0.5$) bromide fraction has been reported for thin films of $MAPb(Br_xI_{1-x})_3$[103,104] and $FAPb(Br_xI_{1-x})_3$[31,32] and attributed to a crystal structure change occurring in this region. As shown in Figure 1b, such low crystallinity leads to a severe "mobility gap"[31] for $FAPb(Br_xI_{1-x})_3$ in the range of bromide fractions $x \sim 0.3$−$0.5$ where values fall below 1 $cm^2/(V\ s)$. However, addition of a small



DOI: 10.1021/acsenergylett.7b00276
ACS Energy Lett. 2017, 2, 1539−1548

quantity of cesium eliminates this gap,[35] resulting in a monotonous decline in charge-carrier mobility with bromide content in $Cs_{0.17}FA_{0.83}Pb(Br_xI_{1-x})_3$ (Figure 1b) as expected from enhanced electron−phonon coupling.[75] Here, addition of cesium serves to stabilize the perovskite phase of $FAPbX_3$ against deterioration into yellow hexagonal or orthorhombic nonperovskite phases, because the effective ionic radius of Cs is smaller than that of FA, which brings the structure closer within the Goldschmidt tolerance range.[35,38,101,102] Interestingly, this approach also appears to make the material more stable against photoinduced halide segregation[35,38] that has been observed for mixed iodide-bromide lead perovskites.[31,104,105] It has therefore been suggested that structural imperfections may act as sites that nucleate such effects.[35]

Charge-carrier mobilties may also be significantly affected in quasi-two-dimensional perovskite structures that incorporate layers of nonconducting organic cations whose size is too large to be accommodated inside the perovskite structure.[106] Two initial studies demonstrated that the incorporation of hydrophobic organic cations such as butylammonium[107] and 2-phenylethylammonium (PEA)[108] resulted in improved moisture resistance of solar cells based on layered lead iodide perovskites. Initial power-conversion efficiencies of such devices did not exceed 8%; however, subsequent improvements in layer orientation yielded increased values,[109,110] commensurate with charge-carrier motion in the perovskite layer plane for which it is not impeded by the insulating cation layers. Similarly, measurements of THz charge-carrier mobilities in thin films of layered lead iodide perovskites $MA_{n-1}PEA_2Pb_nI_{3n+1}$ revealed respectable values around 10 $cm^2/(V\ s)$ when carrier motion was probed within the plane of the perovskite layers.[47] Therefore, such layered perovskites yield high intrinsic in-plane charge-carrier mobilities that can translate into excellent charge extraction, provided that extrinsic parameters such as long-range layer orientation are controlled to result in percolation pathways for charge carriers.

*Summary and Outlook*. Experimental and theoretical evidence suggests that room-temperature charge-carrier mobilities in MHPs are fundamentally limited by Fröhlich interactions between charge carriers and the electric fields associated with LO phonon modes of the ionic lattice. This outcome is not surprising, given that such Fröhlich mechanisms have long been known to dominate the high-temperature regime for many ionic inorganic semiconductors, such as GaAs. For lead-iodide perovskites such as $MAPbI_3$ and $FAPbI_3$, which are currently implemented in the highest-efficiency solar cells, electron and hole mobility values thus appear to be fundamentally limited to at most ~200 $cm^2/(V\ s)$. These values are lower than those for GaAs, reflecting the relatively strong ionicity of the metal-halide bond, the low energy of an LO phonon mode that involves the oscillation of heavy lead atoms, and slightly larger effective charge-carrier masses. Despite this, the suitability of these MHPs for charge extraction remains excellent because the overall charge diffusion length also depends on the charge-recombination lifetimes, which are usually substantially higher than those encountered for typical GaAs.

These considerations allow for predictive trends linking charge-carrier mobilities in MHPs with their composition. For example, an increase in metal-halide ionicity, such as when moving to smaller halides in lead perovskites, will lower charge-carrier mobilities, while substituting a much lighter metal such as tin may increase LO phonon frequencies, allowing higher mobility values. In addition, this outcome suggests that changes in the A-cation are unlikely to yield substantial differences in intrinsic charge-carrier mobility limits, given that the LO phonon is primarily associated with the oscillation of the ionic metal-halide sublattice. While increases in performance have been observed upon the addition of 10−30% of cesium to FA-based lead halide perovskites, these changes primarily result from extrinsic factors, i.e., improvements in crystallinity linked to stabilization of the crystal structure.[35]

Perovskites incorporating lighter metals, such as tin, clearly have excellent potential for high charge-carrier mobilities but are currently mostly limited by extrinsic effects arising from oxidation of $Sn^{2+}$ to $Sn^{4+}$ that causes self-doping. Finding an alternative light metal for the B site that emulates the benign defect chemistry of the lead-based MHPs is the fundamental challenge here. Another class of materials system still affected by extrinsic effects are quasi-two-dimensional, or layered, MHPs. These offer promising protection against degradation through moisture, but reliable control over layer orientation and widths will be essential to ensure that the long-range charge-carrier mobilities are not impeded.

Overall, this Perspective highlights that the best solution-processed or evaporated MHP thin films already reach charge-carrier mobilties that can be within an order of magnitude of the highest theoretically achievable values. This is an extraordinary feat, given the relatively short time period over which MHP thin-film photovoltaics have been pursued.

## AUTHOR INFORMATION


### Corresponding Author

*E-mail: laura.herz@physics.ox.ac.uk.

### ORCID

Laura M. Herz: 0000-0001-9621-334X


### Notes

The author declares no competing financial interest.

### Biography

**Laura Herz** is a Professor of Physics at the University of Oxford. She received her Ph.D. in Physics from the University of Cambridge in 2002 and was a Research Fellow at St John's College Cambridge from 2001 to 2003. Her research interests lie in the area of organic and organic−inorganic hybrid semiconductors including aspects such as self-assembly, nanoscale effects, energy-transfer, and light-harvesting for solar energy conversion.

## ACKNOWLEDGMENTS

The author's research is financially supported by the Engineering and Physical Sciences Research Council UK.

## REFERENCES


(1) Green, M. A.; Emery, K.; Hishikawa, Y.; Warta, W.; Dunlop, E. D.; Levi, D. H.; Ho-Baillie, A. W. Y. Solar Cell Efficiency Tables (Version 49). *Prog. Photovoltaics* **2017**, *25*, 3−13.

(2) Manser, J. S.; Christians, J. A.; Kamat, P. V. Intriguing Optoelectronic Properties of Metal Halide Perovskites. *Chem. Rev.* **2016**, *116*, 12956−13008.

(3) Herz, L. M. Charge Carrier Dynamics in Organic-Inorganic Metal Halide Perovskites. *Annu. Rev. Phys. Chem.* **2016**, *67*, 65−89.

(4) Brenner, T. M.; Egger, D. A.; Kronik, L.; Hodes, G.; Cahen, D. Hybrid Organic-Inorganic Perovskites: Low-Cost Semiconductors With Intriguing Charge-Transport Properties. *Nat. Rev. Mater.* **2016**, *1*, 15007.

(5) Wehrenfennig, C.; Liu, M.; Snaith, H. J.; Johnston, M. B.; Herz, L. M. Homogeneous Emission Line Broadening in the Organo Lead Halide Perovskite $CH_3NH_3PbI_{3-x}Cl_x$. *J. Phys. Chem. Lett.* **2014**, *5*, 1300−1306.




DOI: 10.1021/acsenergylett.7b00276
*ACS Energy Lett.* 2017, 2, 1539−1548

(6) De Wolf, S.; Holovsky, J.; Moon, S.-J.; Löper, P.; Niesen, B.; Ledinsky, M.; Haug, F.-J.; Yum, J.-H.; Ballif, C. Organometal Halide Perovskites: Sharp Optical Absorption Edge And Its Relation to Photovoltaic Performance. *J. Phys. Chem. Lett.* **2014**, *5*, 1035−1039.
(7) Wehrenfennig, C.; Eperon, G. E.; Johnston, M. B.; Snaith, H. J.; Herz, L. M. High Charge Carrier Mobilities and Lifetimes in Organo Lead Trihalide Perovskites. *Adv. Mater.* **2014**, *26*, 1584−1589.
(8) Yin, W.-J.; Shi, T.; Yan, Y. Unusual Defect Physics in $CH_3NH_3PbI_3$ Perovskite Solar Cell Absorber. *Appl. Phys. Lett.* **2014**, *104*, 063903.
(9) Kim, J.; Lee, S.-H.; Lee, J. H.; Hong, K.-H. The Role of Intrinsic Defects in Methylammonium Lead Iodide Perovskite. *J. Phys. Chem. Lett.* **2014**, *5*, 1312−1317.
(10) Stranks, S. D.; Eperon, G. E.; Grancini, G.; Menelaou, C.; Alcocer, M. J. P.; Leijtens, T.; Herz, L. M.; Petrozza, A.; Snaith, H. J. Electron-Hole Diffusion Lengths Exceeding 1 Micrometer in an Organometal Trihalide Perovskite Absorber. *Science* **2013**, *342*, 341−344.
(11) Johnston, M. B.; Herz, L. M. Hybrid Perovskites for Photovoltaics: Charge-Carrier Recombination, Diffusion and Radiative Efficiencies. *Acc. Chem. Res.* **2016**, *49*, 146−154.
(12) Xing, G.; Mathews, N.; Sun, S.; Lim, S. S.; Lam, Y. M.; Grätzel, M.; Mhaisalkar, S.; Sum, T. C. Long-Range Balanced Electron- and Hole-Transport Lengths in Organic-Inorganic $CH_3NH_3PbI_3$. *Science* **2013**, *342*, 344−347.
(13) Liu, M.; Johnston, M. B.; Snaith, H. J. Efficient Planar Heterojunction Perovskite Solar Cells by Vapour Deposition. *Nature* **2013**, *501*, 395−398.
(14) Eperon, G. E.; et al. Perovskite-Perovskite Tandem Photovoltaics With Ideal Bandgaps. *Science* **2016**, *354*, 861−865.
(15) Bi, D.; Yi, C.; Luo, J.; Décoppet, J.-D.; Zhang, F.; Zakeeruddin, S. M.; Li, X.; Hagfeldt, A.; Grätzel, M. Polymer-Templated Nucleation and Crystal Growth of Perovskite Films for Solar Cells With Efficiency Greater Than 21%. *Nat. Energy* **2016**, *1*, 16142.
(16) Brenner, T. M.; Egger, D. A.; Rappe, A. M.; Kronik, L.; Hodes, G.; Cahen, D. Are Mobilities in Hybrid Organic-Inorganic Halide Perovskites Actually "High"? *J. Phys. Chem. Lett.* **2015**, *6*, 4754−4757.
(17) Shi, D.; et al. Low Trap-State Density and Long Carrier Diffusion in Organolead Trihalide Perovskite Single Crystals. *Science* **2015**, *347*, 519−522.
(18) Dong, Q.; Fang, Y.; Shao, Y.; Mulligan, P.; Qiu, J.; Cao, L.; Huang, J. Electron-Hole Diffusion Lengths > 175 $\mu$m in Solution-Grown $CH_3NH_3PbI_3$ Single Crystals. *Science* **2015**, *347*, 967−970.
(19) Milot, R. L.; Eperon, G. E.; Snaith, H. J.; Johnston, M. B.; Herz, L. M. Temperature-Dependent Charge-Carrier Dynamics in $CH_3NH_3PbI_3$. *Adv. Funct. Mater.* **2015**, *25*, 6218−6227.
(20) Ponseca, C. S.; Savenije, T. J.; Abdellah, M.; Zheng, K.; Yartsev, A.; Pascher, T.; Harlang, T.; Chabera, P.; Pullerits, T.; Stepanov, A.; Wolf, J.-P.; Sundström, V. Organometal Halide Perovskite Solar Cell Materials Rationalized: Ultrafast Charge Generation, High and Microsecond-Long Balanced Mobilities and Slow Recombination. *J. Am. Chem. Soc.* **2014**, *136*, 5189−5192.
(21) Hutter, E. M.; Eperon, G. E.; Stranks, S. D.; Savenije, T. J. Charge Carriers in Planar and Meso-Structured Organic-Inorganic Perovskites: Mobilities, Lifetimes, and Concentration of Trap States. *J. Phys. Chem. Lett.* **2015**, *6*, 3082−3090.
(22) Reid, O. G.; Yang, M.; Kopidakis, N.; Zhu, K.; Rumbles, G. Grain-Size-Limited Mobility in Methylammonium Lead Iodide Perovskite Thin Films. *ACS Energy Lett.* **2016**, *1*, 561−565.
(23) Kim, D. H.; Park, J.; Li, Z.; Yang, M.; Park, J.-S.; Park, I. J.; Kim, J. Y.; Berry, J. J.; Rumbles, G.; Zhu, K. 300% Enhancement of Carrier Mobility in Uniaxial-Oriented Perovskite Films Formed by Topotactic-Oriented Attachement. *Adv. Mater.* **2017**, *29*, 1606831.
(24) Guo, Z.; Manser, J. S.; Wan, Y.; Kamat, P. V.; Huang, L. Spatial and Temporal Imaging of Long-Range Charge Transport in Perovskite Thin Films by Ultrafast Microscopy. *Nat. Commun.* **2015**, *6*, 7471.
(25) Saidaminov, M. I.; Abdelhady, A. L.; Murali, B.; Alarousu, E.; Burlakov, V. M.; Peng, W.; Dursun, I.; Wang, L.; He, Y.; Maculan, G.; Goriely, A.; Wu, T.; Mohammed, O. F.; Bakr, O. M. High-Quality Bulk Hybrid Perovskite Single Crystals Within Minutes by Inverse Temperature Crystallization. *Nat. Commun.* **2015**, *6*, 7586.
(26) Valverde-Chavez, D. A.; Ponseca, C. S.; Stoumpos, C. C.; Yartsev, A.; Kanatzidis, M. G.; Sundström, V.; Cooke, D. G. Intrinsic Femtosecond Charge Generation Dynamics in Single Crystal $CH_3NH_3PbI_3$. *Energy Environ. Sci.* **2015**, *8*, 3700−3707.
(27) Semonin, O. E.; Elbaz, G. A.; Straus, D. B.; Hull, T. D.; Paley, D. W.; van der Zande, A. M.; Hone, J. C.; Kymissis, I.; Kagan, C. R.; Roy, X.; Owen, J. S. Limits of Carrier Diffusion in n-Type and p-Type $CH_3NH_3PbI_3$ Perovskite Single Crystals. *J. Phys. Chem. Lett.* **2016**, *7*, 3510−3518.
(28) Stoumpos, C. C.; Malliakas, C. D.; Kanatzidis, M. G. Semiconducting Tin and Lead Iodide Perovskites with Organic Cations: Phase Transitions, High Mobilities, and Near-Infrared Photoluminescent Properties. *Inorg. Chem.* **2013**, *52*, 9019−9038.
(29) Wehrenfennig, C.; Liu, M.; Snaith, H. J.; Johnston, M. B.; Herz, L. M. Charge-Carrier Dynamics in Vapour-Deposited Films of the Organolead Halide Perovskite $CH_3NH_3PbI_{3-x}Cl_x$. *Energy Environ. Sci.* **2014**, *7*, 2269−2275.
(30) Karakus, M.; Jensen, S. A.; D'Angelo, F.; Turchinovich, D.; Bonn, M.; Canovas, E. Phonon-Electron Scattering Limits Free Charge Mobility in Methylammonium Lead Iodide Perovskites. *J. Phys. Chem. Lett.* **2015**, *6*, 4991−4996.
(31) Rehman, W.; Milot, R. L.; Eperon, G. E.; Wehrenfennig, C.; Boland, J. L.; Snaith, H. J.; Johnston, M. B.; Herz, L. M. Charge-Carrier Dynamics and Mobilities in Formamidinium Lead Mixed-Halide Perovskites. *Adv. Mater.* **2015**, *27*, 7938−7944.
(32) Eperon, G. E.; Stranks, S. D.; Menelaou, C.; Johnston, M. B.; Herz, L. M.; Snaith, H. J. Formamidinium Lead Trihalide: a Broadly Tunable Perovskite for Efficient Planar Heterojunction Solar Cells. *Energy Environ. Sci.* **2014**, *7*, 982−988.
(33) Zhumekenov, A. A.; Saidaminov, M. I.; Haque, M. A.; Alarousu, E.; Sarmah, S. P.; Murali, B.; Dursun, I.; Miao, X.-H.; Abdelhady, A. L.; Wu, T.; Mohammed, O. F.; Bakr, O. M. Formamidinium Lead Halide Perovskite Crystals with Unprecedented Long Carrier Dynamics and Diffusion Length. *ACS Energy Lett.* **2016**, *1*, 32−37.
(34) Han, Q.; Bae, S.-H.; Sun, P.; Hsieh, Y.-T.; Yang, Y. M.; Rim, Y. S.; Zhao, H.; Chen, Q.; Shi, W.; Li, G.; Yang, Y. Single Crystal Formamidinium Lead Iodide ($FAPbI_3$): Insight into the Structural, Optical, and Electrical Properties. *Adv. Mater.* **2016**, *28*, 2253−2258.
(35) Rehman, W.; McMeekin, D. P.; Patel, J. B.; Milot, R. L.; Johnston, M. B.; Snaith, H. J.; Herz, L. M. Photovoltaic Mixed-Cation Lead Mixed-Halide Perovskites: Links Between Crystallinity, Photo-Stability and Electronic Properties. *Energy Environ. Sci.* **2017**, *10*, 361−369.
(36) Sheng, R.; Ho-Baillie, A.; Huang, S.; Chen, S.; Wen, X.; Hao, X.; Green, M. A. Methylammonium Lead Bromide Perovskite-Based Solar Cells by Vapor-Assisted Deposition. *J. Phys. Chem. C* **2015**, *119*, 3545−3549.
(37) Maculan, G.; Sheikh, A. D.; Abdelhady, A. L.; Saidaminov, M. I.; Haque, M. A.; Murali, B.; Alarousu, E.; Mohammed, O. F.; Wu, T.; Bakr, O. M. $CH_3NH_3PbCl_3$ Single Crystals: Inverse Temperature Crystallization and Visible-Blind UV-Photodetector. *J. Phys. Chem. Lett.* **2015**, *6*, 3781−3786.
(38) McMeekin, D. P.; Sadoughi, G.; Rehman, W.; Eperon, G. E.; Saliba, M.; Hörantner, M. T.; Haghighirad, A.; Sakai, N.; Korte, L.; Rech, B.; Johnston, M. B.; Herz, L. M.; Snaith, H. J. A Mixed-Cation Lead Mixed-Halide Perovskite Absorber for Tandem Solar Cells. *Science* **2016**, *351*, 151−155.
(39) McMeekin, D. P.; Wang, Z.; Rehman, W.; Pulvirenti, F.; Patel, J. B.; Noel, N. K.; Marder, S. R.; Johnston, M. B.; Herz, L. M.; Snaith, H. J. Crystallization Kinetics and Morphology Control of Mixed-Cation Lead Mixed-Halide Perovskite via Tunability of the Colloidal Precursor Solution. *Adv. Mater.* **2017**, *29*, 1607039.
(40) Noel, N. K.; Stranks, S. D.; Abate, A.; Wehrenfennig, C.; Guarnera, S.; Haghighirad, A. A.; Sadhanala, A.; Eperon, G. E.; Pathak, S. K.; Johnston, M. B.; Petrozza, A.; Herz, L. M.; Snaith, H. J. Lead-Free Organic-Inorganic Tin Halide Perovskites for Photovoltaic Applications. *Energy Environ. Sci.* **2014**, *7*, 3061−3068.
(41) Mitzi, D. B.; Feild, C. A.; Schlesinger, Z.; Laibowitz, R. B. Transport, Optical and Magnetic Properties of the Conducting Halide Perovskite $CH_3NH_3SnI_3$. *J. Solid State Chem.* **1995**, *114*, 159−163.


DOI: 10.1021/acsenergylett.7b00276
*ACS Energy Lett.* 2017, 2, 1539−1548

(42) Takahashi, Y.; Hasegawa, H.; Takahashi, Y.; Inabe, T. Hall Mobility in Tin Iodide Perovskite $CH_3NH_3SnI_3$: Evidence for a Doped Semiconductor. *J. Solid State Chem.* **2013**, *205*, 39−43.
(43) Milot, R. L.; Eperon, G. E.; Green, T.; Snaith, H. J.; Johnston, M. B.; Herz, L. M. Radiative Monomolecular Recombination Boosts Amplified Spontaneous Emission in $HC(NH_2)_2SnI_3$ Perovskite Films. *J. Phys. Chem. Lett.* **2016**, *7*, 4178−4184.
(44) Chung, I.; Song, J.-H.; Im, J.; Androulakis, J.; Malliakas, C. D.; Li, H.; Freeman, A. J.; Kenney, J. T.; Kanatzidis, M. G. $CsSnI_3$: Semiconductor or Metal? High Electrical Conductivity and Strong Near-Infrared Photoluminescence from a Single Material. High Hole Mobility and Phase-Transitions. *J. Am. Chem. Soc.* **2012**, *134*, 8579−8587.
(45) Kagan, C. R.; Mitzi, D. B.; Dimitrakopoulos, C. D. Organic-Inorganic Hybrid Materials as Semiconducting Channels in Thin-Film Field-Effect Transistors. *Science* **1999**, *286*, 945−947.
(46) Matsushima, T.; Hwang, S.; Sandanayaka, A. S. D.; Qin, C.; Terakawa, S.; Fujihara, T.; Yahiro, M.; Adachi, C. Solution-Processed Organic-Inorganic Perovskite Field-Effect Transistors with High Hole Mobilities. *Adv. Mater.* **2016**, *28*, 10275−10281.
(47) Milot, R. L.; Sutton, R. J.; Eperon, G. E.; Haghighirad, A. A.; Hardigree, J. M.; Miranda, L.; Snaith, H. J.; Johnston, M. B.; Herz, L. M. Charge-Carrier Dynamics in 2D Hybrid Metal-Halide Perovskites. *Nano Lett.* **2016**, *16*, 7001−7007.
(48) Eames, C.; Frost, J. M.; Barnes, P. R. F.; O'Regan, B. C.; Walsh, A.; Islam, M. S. Ionic Transport in Hybrid Lead Iodide Perovskite Solar Cells. *Nat. Commun.* **2015**, *6*, 7497.
(49) Chen, B.; Yang, M.; Zheng, X.; Wu, C.; Li, W.; Yan, Y.; Bisquert, J.; Garcia-Belmonte, G.; Zhu, K.; Priya, S. Impact of Capacitive Effect and Ion Migration on the Hysteretic Behavior of Perovskite Solar Cells. *J. Phys. Chem. Lett.* **2015**, *6*, 4693−4700.
(50) Christians, J. A.; Leighton, D. T.; Kamat, P. V. Rate Limiting Interfacial Hole Transfer in $Sb_2S_3$ Solid-State Solar Cells. *Energy Environ. Sci.* **2014**, *7*, 1148−1158.
(51) Oga, H.; Saeki, A.; Ogomi, Y.; Hayase, S.; Seki, S. Improved Understanding of the Electronic and Energetic Landscapes of Perovskite Solar Cells: High Local Charge Carrier Mobility, Reduced Recombination, and Extremely Shallow Traps. *J. Am. Chem. Soc.* **2014**, *136*, 13818−13825.
(52) Savenije, T. J.; Ponseca, C. S.; Kunneman, L.; Abdellah, M.; Zheng, K.; Tian, Y.; Zhu, Q.; Canton, S. E.; Scheblykin, I. G.; Pullerits, T.; Yartsev, A.; Sundström, V. Thermally Activated Exciton Dissociation and Recombination Control the Carrier Dynamics in Organometal Halide Perovskite. *J. Phys. Chem. Lett.* **2014**, *5*, 2189−2194.
(53) Yu, P. Y.; Cardona, M. *Fundamentals of Semiconductors*, 1st ed.; Springer: New York, 1996.
(54) Chang, Y. H.; Park, C. H.; Matsuishi, K. First-Principles Study of the Structural and the Electronic Properties of the Lead-Halide-Based Inorganic-Organic Perovskites $(CH_3NH_3)PbX_3$ and $CsPbX_3$ (X = Cl, Br, I). *J. Korean Phys. Soc.* **2004**, *44*, 889−893.
(55) Menendez-Proupin, E.; Palacios, P.; Wahnon, P.; Conesa, J. C. Self-Consistent Relativistic Band Structure of the $CH_3NH_3PbI_3$. *Phys. Rev. B: Condens. Matter Mater. Phys.* **2014**, *90*, 045207.
(56) Giorgi, G.; Fujisawa, J.-I.; Segawa, H.; Yamashita, K. Small Photocarrier Effective Masses Featuring Ambipolar Transport in Methylammonium Lead Iodide Perovskite: A Density Functional Analysis. *J. Phys. Chem. Lett.* **2013**, *4*, 4213−4216.
(57) Umari, P.; Mosconi, E.; de Angelis, F. Relativistic GW Calculations on $CH_3NH_3PbI_3$ and $CH_3NH_3SnI_3$ Perovskites for Solar Cell Applications. *Sci. Rep.* **2015**, *4*, 4467.
(58) Brivio, F.; Butler, K. T.; Walsh, A.; van Schilfgaarde, M. Relativistic Quasiparticle Self-Consistent Electronic Structure of Hybrid Halide Perovskite Photovoltaic Absorbers. *Phys. Rev. B: Condens. Matter Mater. Phys.* **2014**, *89*, 155204.
(59) Motta, C.; El-Mellouhi, F.; Sanvito, S. Charge Carrier Mobility in Hybrid Halide Perovskites. *Sci. Rep.* **2015**, *5*, 12746.
(60) Tanaka, K.; Takahashi, T.; Ban, T.; Kondo, T.; Uchida, K.; Miura, N. Comparative Study on the Excitons in Lead-Halide-Based Perovskite-Type Crystals $CH_3NH_3PbBr_3$ $CH_3NH_3PbI_3$. *Solid State Commun.* **2003**, *127*, 619−623.
(61) Hirasawa, M.; Ishihara, T.; Goto, T.; Uchida, K.; Miura, N. Magnetoabsorption of the Lowest Exciton in Perovskite-Type Compound $(CH_3NH_3)PbI_3$. *Phys. B* **1994**, *201*, 427−430.
(62) Miyata, A.; Mitioglu, A.; Plochocka, P.; Portugall, O.; Wang, J. T.-W.; Stranks, S. D.; Snaith, H. J.; Nicholas, R. J. Direct Measurement of the Exciton Binding Energy and Effective Masses for Charge Carriers in an Organic-Inorganic Tri-Halide Perovskite. *Nat. Phys.* **2015**, *11*, 582−587.
(63) Galkowski, K.; Mitioglu, A.; Miyata, A.; Plochocka, P.; Portugall, O.; Eperon, G. E.; Wang, J. T.-W.; Stergiopoulos, T.; Stranks, S. D.; Snaith, H. J.; Nicholas, R. J. Determination of the Exciton Binding Energy and Effective Masses for Methylammonium and Formamidinium Lead Tri-Halide Perovskite Semiconductors. *Energy Environ. Sci.* **2016**, *9*, 962−970.
(64) Amat, A.; Mosconi, E.; Ronca, E.; Quarti, C.; Umari, P.; Nazeeruddin, M. K.; Grätzel, M.; De Angelis, F. Cation-Induced Band-Gap Tuning in Organohalide Perovskites: Interplay of Spin-Orbit Coupling and Octahedra Tilting. *Nano Lett.* **2014**, *14*, 3608−3616.
(65) Sotoodeh, M.; Khalid, A. H.; Rezazadeh, A. A. Empirical Low-Field Mobility Model for III-V Compounds Applicable in Device Simulation Codes. *J. Appl. Phys.* **2000**, *87*, 2890.
(66) Seitz, F. On the Mobility of Electrons in Pure Non-Polar Insulators. *Phys. Rev.* **1948**, *73*, 549−564.
(67) Bardeen, J.; Shockley, W. Deformation Potentials and Mobilities in Non-Polar Crystals. *Phys. Rev.* **1950**, *80*, 72−80.
(68) Fröhlich, H. Electrons in Lattice Fields. *Adv. Phys.* **1954**, *3*, 325−361.
(69) Feynman, R. P. Slow Electrons in a Polar Crystal. *Phys. Rev.* **1955**, *97*, 660−665.
(70) Even, J.; Paofai, S.; Bourges, P.; Letoublon, A.; Cordier, S.; Durand, O.; Katan, C. Carrier Scattering Processes and Low Energy Phonon Spectroscopy in Hybrid Perovskite Crystals. *Proc. SPIE* **2016**, *9743*, 97430M.
(71) Neukirch, A. J.; Nie, W.; Blancon, J.-S.; Appavoo, K.; Tsai, H.; Sfeir, M. Y.; Katan, C.; Pedesseau, L.; Even, J.; Crochet, J. J.; Gupta, G.; Mohite, A. D.; Tretiak, S. Polaron Stabilization by Cooperative Lattice Distortion and Cation Rotations in Hybrid Perovskite Materials. *Nano Lett.* **2016**, *16*, 3809−3816.
(72) He, Y.; Galli, G. Perovskites for Solar Thermoelectric Applications: A First Principle Study of $CH_3NH_3AI_3$ (A = Pb and Sn). *Chem. Mater.* **2014**, *26*, 5394−5400.
(73) Wang, Y.; Zhang, Y.; Zhang, P.; Zhang, W. High Intrinsic Carrier Mobility and Photon Absorption in the Perovskite $CH_3NH_3PbI_3$. *Phys. Chem. Chem. Phys.* **2015**, *17*, 11516−11520.
(74) Yu, Z.-G. Rashba Effect and Carrier Mobility in Hybrid Organic-Inorganic Perovskites. *J. Phys. Chem. Lett.* **2016**, *7*, 3078−3083.
(75) Wright, A. D.; Verdi, C.; Milot, R. L.; Eperon, G. E.; Pérez-Osorio, M. A.; Snaith, H. J.; Giustino, F.; Johnston, M. B.; Herz, L. M. Electron-Phonon Coupling in Hybrid Lead Halide Perovskites. *Nat. Commun.* **2016**, *7*, 11755.
(76) Filippetti, A.; Mattoni, A.; Caddeo, C.; Saba, M. I.; Delugas, P. Low Electron-Polar Optical Phonon Scattering as a Fundamental Aspect of Carrier Mobility in Methylammonium Lead Halide $CH_3NH_3PbI_3$ Perovskites. *Phys. Chem. Chem. Phys.* **2016**, *18*, 15352−15362.
(77) Sendner, M.; Nayak, P. K.; Egger, D. A.; Beck, S.; Müller, C.; Epding, B.; Kowalsky, W.; Kronik, L.; Snaith, H. J.; Pucci, A.; Lovrincic, R. Optical Phonons in Methylammonium Lead Halide Perovskites and Implications for Charge Transport. *Mater. Horiz.* **2016**, *3*, 613−620.
(78) Whalley, L. D.; Skelton, J. M.; Frost, J. M.; Walsh, A. Phonon Anharmonicity, Lifetimes, and Thermal Transport in $CH_3NH_3PbI_3$ From Many-Body Perturbation Theory. *Phys. Rev. B: Condens. Matter Mater. Phys.* **2016**, *94*, 220301.
(79) Letoublon, A.; Paofai, S.; Ruffle, B.; Bourges, P.; Hehlen, B.; Michel, T.; Ecolivet, C.; Durand, O.; Cordier, S.; Katan, C.; Even, J. Elastic Constants, Optical Phonons, and Molecular Relaxations in the High Temperature Plastic Phase of the $CH_3NH_3PbBr_3$ Hybrid Perovskite. *J. Phys. Chem. Lett.* **2016**, *7*, 3776−3784.


DOI: 10.1021/acsenergylett.7b00276
*ACS Energy Lett.* 2017, 2, 1539−1548

(80) Wehrenfennig, C.; Liu, M.; Snaith, H. J.; Johnston, M. B.; Herz, L. M. Charge Carrier Recombination Channels in the Low-Temperature Phase of Organic-Inorganic Lead Halide Perovskite Thin Films. *APL Mater.* **2014**, *2*, 081513.
(81) Perez-Osorio, M. A.; Milot, R. L.; Filip, M. R.; Patel, J. B.; Herz, L. M.; Johnston, M. B.; Giustino, F. Vibrational Properties of the Organic-Inorganic Halide Perovskite $CH_3NH_3PbI_3$ from Theory and Experiment: Factor Group Analysis, First-Principles Calculations, and Low-Temperature Infrared Spectra. *J. Phys. Chem. C* **2015**, *119*, 25703.
(82) Frost, J. M. Polaron Mobility in Halide Perovskites. 2017, arXiv:1704.05404 [cond-mat.mtrl-sci].
(83) Stillman, G. E.; Wolfe, C. M.; Dimmock, J. O. Hall Coefficient Factor for Polar Mode Scattering in n-Type GaAs. *J. Phys. Chem. Solids* **1970**, *31*, 1199−1204.
(84) Benavides-Garcia, M.; Balasubramanian, K. Bond Energies, Ionization Potentials, and the Singlet-Triplet Energy Separations of $SnCl_2$, $SnBr_2$, $SnI_2$, $PbCl_2$, $PbBr_2$, $PbI_2$, and Their Positive Ions. *J. Chem. Phys.* **1994**, *100*, 2821−2830.
(85) Waugh, J. L. T.; Dolling, G. Crystal Dynamics of Gallium Arsenide. *Phys. Rev.* **1963**, *132*, 2410−2412.
(86) Biaggio, I.; Hellwarth, R. W.; Partanen, J. P. Band Mobility of Photoexcited Electroncs in $Bi_{12}SiO_{20}$. *Phys. Rev. Lett.* **1997**, *78*, 891−894.
(87) Hellwarth, R. W.; Biaggio, I. Mobility of an Electron in a Multimode Polar Lattice. *Phys. Rev. B: Condens. Matter Mater. Phys.* **1999**, *60*, 299−307.
(88) Feynman, R. P.; Hellwarth, R. W.; Iddings, C. K.; Platzman, P. M. Mobility of Slow Electrons in a Polar Crystal. *Phys. Rev.* **1962**, *127*, 1004−1017.
(89) Edri, E.; Kirmayer, S.; Henning, A.; Mukhopadhyay, S.; Gartsman, K.; Rosenwaks, Y.; Hodes, G.; Cahen, D. Why Lead Methylammonium Tri-Iodide Perovskite-Based Solar Cells Require a Mesoporous Electron Transporting Scaffold (but Not Necessarily a Hole Conductor). *Nano Lett.* **2014**, *14*, 1000−1004.
(90) Dar, M.; Arora, N.; Gao, P.; Ahmad, S.; Grätzel, M.; Nazeeruddin, M. K. Investigation Regarding the Role of Chloride in Organic-Inorganic Halide Perovskites Obtained from Chloride Containing Precursors. *Nano Lett.* **2014**, *14*, 6991−6996.
(91) Colella, S.; Mosconi, E.; Fedeli, P.; Listorti, A.; Gazza, F.; Orlandi, F.; Ferro, P.; Besagni, T.; Rizzo, A.; Calestani, G.; Gigli, G.; Angelis, F. D.; Mosca, R. $MAPbI_{3x}Cl_x$ Mixed Halide Perovskite for Hybrid Solar Cells: The Role of Chloride as Dopant on the Transport and Structural Properties. *Chem. Mater.* **2013**, *25*, 4613−4618.
(92) Parrott, E. S.; Milot, R. L.; Stergiopoulos, T.; Snaith, H. J.; Johnston, M. B.; Herz, L. M. Effect of Structural Phase Transition on Charge-Carrier Lifetimes and Defects in $CH_3NH_3SnI_3$ Perovskite. *J. Phys. Chem. Lett.* **2016**, *7*, 1321−1326.
(93) Störmer, H.; Dingle, R.; Gossard, A.; Wiegmann, W.; Sturge, M. Two-Dimensional Electron Gas at a Semiconductor-Semiconductor Interface. *Solid State Commun.* **1979**, *29*, 705−709.
(94) Boland, J. L.; Conesa-Boj, S.; Parkinson, P.; Tütüncüoglu, G.; Matteini, F.; Rüffer, D.; Casadei, A.; Amaduzzi, F.; Jabeen, F.; Davies, C. L.; Joyce, H. J.; Herz, L. M.; i Morral, A. F.; Johnston, M. B. Modulation Doping of GaAs/AlGaAs Core-Shell Nanowires With Effective Defect Passivation and High Electron Mobility. *Nano Lett.* **2015**, *15*, 1336.
(95) Kumar, M. H.; Dharani, S.; Leong, W. L.; Boix, P. P.; Prabhakar, R. R.; Baikie, T.; Ding, C. S. H.; Ramesh, R.; Asta, M.; Grätzel, M.; Mhaisalkar, S. G.; Mathews, N. Lead-Free Halide Perovskite Solar Cells with High Photocurrents Realized Through Vacancy Modulation. *Adv. Mater.* **2014**, *26*, 7122−7127.
(96) Lee, S. J.; Shin, S. S.; Kim, Y. C.; Kim, D.; Ahn, T. K.; Noh, J. H.; Seo, J.; Seok, S. I. Fabrication of Efficient Formamidinium Tin Iodide Perovskite Solar Cells through $SnF_2$-Pyrazine Complex. *J. Am. Chem. Soc.* **2016**, *138*, 3974−3977.
(97) Wang, Q.; Shao, Y.; Xie, H.; Lyu, L.; Liu, X.; Gao, Y.; Huang, J. Qualifying Composition Dependent p and n Self-Doping in $CH_3NH_3PbI_3$. *Appl. Phys. Lett.* **2014**, *105*, 163508.
(98) Siebentritt, S.; Rey, G.; Finger, A.; Regesch, D.; Sendler, J.; Weiss, T. P.; Bertram, T. What Is the Bandgap of Kesterite? *Sol. Energy Mater. Sol. Cells* **2016**, *158*, 126−129.
(99) Gokmen, T.; Gunawan, O.; Todorov, T. K.; Mitzi, D. B. Band Tailing and Efficiency Limitation in Kesterite Solar Cells. *Appl. Phys. Lett.* **2013**, *103*, 103506.
(100) Goldschmidt, V. M. Die Gesetze der Krystallochemie. *Naturwissenschaften* **1926**, *14*, 477−485.
(101) Li, Z.; Yang, M.; Park, J.-S.; Wei, S.-H.; Berry, J. J.; Zhu, K. Stabilizing Perovskite Structures by Tuning Tolerance Factor: Formation of Formamidinium and Cesium Lead Iodide Solid-State Alloys. *Chem. Mater.* **2016**, *28*, 284−292.
(102) Saliba, M.; Matsui, T.; Seo, J.-Y.; Domanski, K.; Correa-Baena, J.-P.; Nazeeruddin, M. K.; Zakeeruddin, S. M.; Tress, W.; Abate, A.; Hagfeldt, A.; Grätzel, M. Cesium-Containing Triple Cation Perovskite Solar Cells: Improved Stability, Reproducibility and High Efficiency. *Energy Environ. Sci.* **2016**, *9*, 1989−1997.
(103) Sadhanala, A.; Deschler, F.; Thomas, T. H.; Dutton, S. E.; Goedel, K. C.; Hanusch, F. C.; Lai, M. L.; Steiner, U.; Bein, T.; Docampo, P.; Cahen, D.; Friend, R. H. Preparation of Single-Phase Films of $CH_3NH_3Pb(I_{1-x}Br_x)_3$ With Sharp Optical Band Edges. *J. Phys. Chem. Lett.* **2014**, *5*, 2501−2505.
(104) Hoke, E. T.; Slotcavage, D. J.; Dohner, E. R.; Bowring, A. R.; Karunadasa, H. I.; McGehee, M. D. Reversible Photo-Induced Trap Formation in Mixed-Halide Hybrid Perovskites for Photovoltaics. *Chem. Sci.* **2015**, *6*, 613−617.
(105) Yoon, S. J.; Draguta, S.; Manser, J. S.; Sharia, O.; Schneider, W. F.; Kuno, M.; Kamat, P. V. Tracking Iodide and Bromide Ion Segregation in Mixed Halide Lead Perovskites during Photoirradiation. *ACS Energy Lett.* **2016**, *1*, 290−296.
(106) Mitzi, D. B.; Chondroudis, K.; Kagan, C. Organic-Inorganic Electronics. *IBM J. Res. Dev.* **2001**, *45*, 29.
(107) Cao, D. H.; Stoumpos, C. C.; Farha, O. K.; Hupp, J. T.; Kanatzidis, M. G. 2D Homologous Perovskites as Light-Absorbing Materials for Solar Cell Applications. *J. Am. Chem. Soc.* **2015**, *137*, 7843−7850.
(108) Smith, I. C.; Hoke, E. T.; Solis-Ibarra, D.; McGehee, M. D.; Karunadasa, H. I. A Layered Hybrid Perovskite Solar-Cell Absorber With Enhanced Moisture Stability. *Angew. Chem., Int. Ed.* **2014**, *53*, 11232−11235.
(109) Tsai, H.; et al. High-Efficiency Two-Dimensional Ruddlesden-Popper Perovskite Solar Cells. *Nature* **2016**, *536*, 312−316.
(110) Koh, T. M.; Shanmugam, V.; Schlipf, J.; Oesinghaus, L.; Müller-Buschbaum, P.; Ramakrishnan, N.; Swamy, V.; Mathews, N.; Boix, P. P.; Mhaisalkar, S. G. Nanostructuring Mixed-Dimensional Perovskites: A Route Toward Tunable, Efficient Photovoltaics. *Adv. Mater.* **2016**, *28*, 3653.


DOI: 10.1021/acsenergylett.7b00276
*ACS Energy Lett.* 2017, 2, 1539−1548